Supporting Information

Due et al. 10.1073/pnas.1015996108

SI Materials and Methods.

Expression and Purification. The open reading frame of *priA* from *Mycobacterium tuberculosis* (Rv1603) was amplified by PCR from *M. tuberculosis* chromosomal DNA and cloned into the pETM-11 vector, which contains an N-terminal polyhistidine tag, followed by a tobacco etch virus (TEV) protease cleavage site. Residue point mutations were introduced with the QuikChange site-directed mutagenesis kit (Stratagene) and verified by double-stranded sequencing. All wild-type and mutant PriA variants were heterologously expressed in *Escherichia coli* BL21 Star (DE3) pLysS in ZYM 5052 autoinduction medium (1) at 20 °C. The cells were harvested after reaching saturation, resuspended in lysis buffer (50 mM Tris-HCl, 300 mM NaCl, 20 mM imidazole, 0.2% (vol/vol) NP-40, 0.02% (vol/vol) 1-thioglycerol, pH 8.0), and lysed by sonication for 3 min on ice. The lysate was centrifuged at $38,720 \times g$ for 1 h using a SS-34 rotor in a Sorvall RC26 Plus centrifuge and the supernatant was applied to a 5-mL HiTrap Chelating Sepharose column (GE Healthcare), which was preequilibrated in buffer A (50 mM Tris-HCl, 300 mM NaCl, 20 mM imidazole, 0.01% (vol/vol) 1-thioglycerol, pH 8.0). After washing with 10 column volumes of buffer A, bound proteins were eluted with buffer B (50 mM Tris-HCl, 300 mM NaCl, 300 mM imidazole, 0.01% (vol/vol) 1-thioglycerol, pH 8.0). The sample was subsequently subjected to size exclusion chromatography using a HiLoad 16/60 Superdex 200 column (GE Healthcare), which was equilibrated in buffer C (50 mM Tris-HCl, 300 mM NaCl, and 0.01% (vol/vol) 1-thioglycerol, pH 8.0). The elution peak containing monomeric wild-type or mutant PriA variant was collected. Protein samples for X-ray crystallography were incubated overnight with TEV protease in a 1:50 molar ratio at 4 °C. TEV-cleaved protein was further purified by affinity chromatography using a 5-mL HiTrap Chelating Sepharose column. The protein was subsequently concentrated with a centrifugal concentrator (Vivascience) to 10 mg/mL, flash frozen in liquid nitrogen and stored at −80 °C. Other protein samples were concentrated directly after size exclusion chromatography to approx. 5 mg/mL, flash frozen in liquid nitrogen and stored at −80 °C.

The expression constructs pET21-tmHisA (2) and pET11-tmTrpF (3) were used for the production of *Thermotoga maritima* HisA and TrpF. To simplify purification of TrpF, the *trpF* gene was amplified by PCR from its construct and cloned into the pETM-11 expression vector. Both proteins were expressed in *E. coli* BL21 (DE3) in ZYM 5052 medium (1) at 20 °C. The cells were harvested, lysed, and the proteins purified, as described for PriA. The HisA and TrpF samples were concentrated after size exclusion chromatography to 8.5 and 5.0 mg/mL, respectively, flash frozen in liquid nitrogen, and stored at −80 °C.

Crystallization and X-ray Structure Determination. All PriA crystals were grown by vapor diffusion experiments. Initial conditions were identified, using the local automated crystallization facility (4). PriA(D11N) without additional ligands was crystallized by mixing 300 μM (8 mg/mL) PriA and a reservoir solution containing 2.0 M ammonium sulfate in 0.1 M Bis-Tris (pH 7.5) buffer in a 1:1 ratio. For cocrystallization experiments, ProFAR and rCdRP were prepared by previously described procedures (5, 6). Drops containing 300 μM (8 mg/mL) PriA were mixed with either 5 mM ProFAR or 5 mM rCdRP and mixed 1:1 with the reservoir solution. PriA crystals in the presence of ProFAR were obtained from 1.4 M tri-sodium citrate dihydrate in 0.1 M Hepes (pH 7.5) buffer. PriA crystals in the presence of rCdRP were grown from 32% (wt/vol) PEG 6000 in 0.1 M sodium acetate buffer (pH 5.7).

X-ray data were collected at the synchrotron radiation beamlines X13 (European Molecular Biology Laboratory/Deutsches Elektronen Synchrotron) and BM14 (European Synchrotron Radiation Facility). All crystals were cryoprotected with 25% (vol/vol) glycerol in reservoir solution before they were flash-cooled directly in the cryo stream. The data were indexed and processed with either MOSFLM (7), SCALA (8), or the XDS package (9). Initial phases for each X-ray dataset were obtained by molecular replacement using MOLREP (10). The coordinates of the PriA structure from *Streptomyces coelicolor* (PDB ID code 1VZW) were used as a model to determine the structure of the PriA-rCdRP complex. For subsequent structure determinations (PriA-PrFAR, PriA-apo), the refined structure of the PriA-rCdRP complex was used as a starting model.

All structures were refined using REFMAC (11). In the crystal form comprising the PriA-rCdRP complex, there were four molecules within each asymmetric unit. Refinement of this structure was carried out with the Translation Libration Screw option in REFMAC (12). Chain C of the PriA-rCdRP complex was selected for further structural/functional interpretation. During the final rounds of the refinement of the PriA-PrFAR complex, the structural models were refined using an anisotropic B-factor model. The high resolution of the PriA-PrFAR complex enabled us to model PriA residues Gln22, Val35, Arg116, Glu120, Gln134, Glu146, Ser161, Thr173, Leu186, Thr216, and PrFAR atoms C7, C1", C2", N8, O2 with alternate conformations. In all PriA structures, only those sequence segments with sufficient electron density were modeled. PriA-apo: 2-143 and 148-245; PriA-rCdRP: chain A, 2-19 and 29-244; chain B, 2-21 and 29-244; chain C, 2-19 and 30-244; chain D, 2-20 and 30-244; PriA-PrFAR, 2-245. Those residues with insufficient side-chain electron density were modeled as alanine residues: PriA-apo: Asp135, Arg141, Lys174, Asp175, Thr177, Leu178; PriA-rCdRP: chain A, Thr29, Glu30; chain B, Thr29, Glu30, Val 31; chain C, Glu30; chain D, Leu20. In the PriA-PrFAR complex, PrFAR and the following PriA residues were modeled with two alternative conformations: Gln22, Val35, Arg116, Glu120, Gln134, Glu146, Ser161, Thr173, Leu186, Thr216. The overall data collection and refinement statistics are given in Table S1.

Comparison of the PriA-sulfate complex (apo) from *M. tuberculosis* with those of the same enzyme from *S. coelicolor* in the presence of sulfate (13, 14) reveals no significant changes of the overall fold and active site loop structure (1VZW, root mean squares deviation = 0.91 Å; 1VEP, root mean squares deviation = 1.07 Å), indicating that the conformational changes observed in the two PriA-ligand complexes are caused by the presence of the reaction ligands.

Steady-State Kinetics. ProFAR isomerization activity of the PriA variants was measured as described (5). In each PriA single-residue mutant, we removed the side chain-specific function by changing the respective amino acid into an alanine. Those residues, where we were not able to detect any catalytic activity of the PriA alanine variant, were also changed into the most closely related amino acid (Fig. 3 and Table S2). The reaction was performed in the presence of an excess of the cyclase (HisF) subunit of imidazole glycerol phosphate synthase from *T. maritima* in assay buffer (50 mM Tris, 100 mM ammonium acetate, pH 8.5), to enzymatically remove the product PrFAR, thus excluding potential product inhibition. The ProFAR isomerization reaction was followed by measuring the decrease of the absorbance at 300 nm. The amount of substrate reacted was calculated using

a specific extinction coefficient difference (ProFAR—AICAR) of 5637 M^{-1} cm^{-1} at 300 nm. The assay was performed in 96 well microtitre plates using six concentrations of ProFAR (10, 20, 40, 80, 160, and 320 μM) for each PriA variant. The concentration of wild-type and mutant PriA variants used in the assay were 0.6 μM and 5–50 μM, respectively. The assays were performed using a PowerWave spectrophotometer (BioTek Instruments) at 30 °C. Catalytic constants, K_M^{ProFAR} and k_{cat}, were derived from plotting the initial enzymatic velocities against the initial ProFAR concentration and applying Michaelis–Menten kinetics.

Phosphoribosyl anthranilate (PRA) isomerization of the PriA variants was performed as described (15). The first step of the assay is the conversion of anthranilic acid into PRA by anthranilate phosphoribosyltransferase (TrpD) from yeast, in the presence of a large molar excess of phosphoribosyl pyrophosphate. The reaction was followed by the decrease in fluorescence emission at 400 nm, after excitation at 350 nm. The conversion was completed when a constant fluorescence intensity was obtained. In the second step of the assay, purified PriA was added to the reaction mixture. The subsequent PriA catalyzed conversion of PRA to CdRP was followed by a further decrease in fluorescence emission using the same settings. Wild-type PriA was used in a concentration of 100 to 400 nM, whereas the PriA mutants were used in a concentration range of 200 nM to 10 μM, depending on the activity level. The reactions were performed in 1-mL cuvettes in a Flourolog spectrometer (Horiba Jobin Yvon) at 30 °C. Each PriA variant was measured using several substrate concentrations (10, 20, 40, and 80 μM). The resulting kinetic curves were fitted with the software COSY v5.5 to obtain the kinetic constants k_{cat} and K_M^{PRA} (16).

Identification and Characterization of PriA Inhibitors. A search for potential PriA inhibitors was performed using a library of 20,000 small molecule compounds, available at Leibniz-Institute for Molecular Pharmacology. Screens were performed in 384 well microtiter plates, using the established ProFAR isomerization activity assay (5). Each compound was tested at a concentration of 50 μM, in the presence of 25 μM ProFAR and 150 nM wild-type PriA. For each plate, two columns were used for positive controls (no compound added) and negative control (no PriA added). The reactions were started by mechanically dispensing substrate solution to all wells of each microtiter plate. The reaction velocity was thereafter monitored, by measuring the decrease in absorbance at 300 nm with a Safire II spectrophotometer (Tecan). A total of 20 compounds that inhibited more than 50% PriA activity were considered as initial positive hits.

These compounds were further assessed, by repeating the measurements of each compound at three concentrations (25 μM, 50 μM, and 100 μM) and two ProFAR concentrations (25 μM and 50 μM). From these data, false positive hits were identified by concentration independent inhibition and excluded from further analyses. To assess the efficacy against the bisubstrate properties of PriA, the remaining positive hits were subsequently tested for inhibition of the second PriA activity, PRA isomerization. The measurements were performed with 16 μM PRA and each compound at three concentrations (25 μM, 50 μM, and 100 μM). The inhibitor concentrations leading to 50% of the maximal inhibition (IC50) for both activities were estimated on the basis of these measurements.

Selected inhibitors

- (E)-N-(3-chloro-5-methyl-4-oxocyclohexa-2,5-dienylidene) benzenesulfonamide, #16827, 3993-4586, Chem-Div
- 2,5-dimethyl-N-(4-oxocyclohexa-2,5-dienylidene)benzenesulfonamide #17146, 4456-2380, Chem-Div
- 3-(allylamino)-4-chloro-1-(2-chlorophenyl)-1H-pyrrole-2,5-dione #19746, 3232-1872, Chem-Div
- 3,6-Dihydroxybenzo-norborane, #20022, 16643, Acros Organics
- (Z)-2-(5-(1-benzyl-5-bromo-2-oxoindolin-3-ylidene)-4-oxo-2-thioxothiazolidin-3-yl)ethanesulfonic acid, #20138, PHAR055248, Pharmeks
- 2-heptadecyl-3-[(2-hydroxy-5-sulfophenyl)diazenyl]-3H-pyrazolo[1,5-a]benzimidazole-6-sulfonic acid #20169, AH-034/08462005, Specs

For quantitative determination of the inhibition constants of the selected compounds, the ProFAR and PRA isomerization activities of PriA were assessed in the presence of inhibitors at different concentrations in microtitre plates. Catalytic turnover of ProFAR and PRA was measured using a PowerWave spectrophotometer (BioTek Instruments) and on a Safire II fluorescence spectrophotometer (Tecan) at 30 °C, respectively. In the ProFAR isomerization assay, six concentrations of ProFAR (10, 20, 40, 80, 160, and 320 μM) were used in the presence 500 nM wild-type PriA. For the PRA isomerization assay, solutions with five concentrations of PRA (2.5, 5, 10, 20, and 40 μM) were prepared from equal amounts of anthranilic acid and added to the well microtitre plates, containing 200 nM PriA. Each inhibitor was evaluated using two or more concentrations, in accordance with the estimated IC50 values. The inhibition constant (K_i) and the type of inhibition were determined by fitting the obtained experimental data simultaneously to equations for the different types of inhibition possible (competitive, noncompetitive or mixed), using the IGOR software, version 4.0 (WaveMetrics). The inhibition properties for HisA and TrpF from *Thermotoga maritima* were analyzed analogously with enzyme concentrations of 75 nM and 150 nM, respectively.

1. Studier FW (2005) Protein production by auto-induction in high density shaking cultures. *Protein Expres Purif* 41:207–234.
2. Thoma R, et al. (1999) Efficient expression, purification and crystallisation of two hyperthermostable enzymes of histidine biosynthesis. *FEBS Lett* 454:1–6.
3. Thoma R, Hennig M, Sterner R, Kirschner K (2000) Structure and function of mutationally generated monomers of dimeric phosphoribosylanthranilate isomerase from Thermotoga maritima. *Structure* 8:265–276.
4. Mueller-Dieckmann J (2006) The open-access high-throughput crystallization facility at EMBL Hamburg. *Acta Crystallogr D* 62:1446–1452.
5. Klem TJ, Davisson VJ (1993) Imidazole glycerol phosphate synthase: The glutamine amidotransferase in histidine biosynthesis. *Biochemistry* 32:5177–5186.
6. Henn-Sax M, et al. (2002) Two (betaalpha)(8)-barrel enzymes of histidine and tryptophan biosynthesis have similar reaction mechanisms and common strategies for protecting their labile substrates. *Biochemistry* 41:12032–12042.
7. Leslie AG (2006) The integration of macromolecular diffraction data. *Acta Crystallogr D* 62:48–57.
8. Evans P (2006) Scaling and assessment of data quality. *Acta Crystallogr D* 62:72–82.
9. Kabsch W (1993) Automatic processing of rotation diffraction data from crystals of initially unknown symmetry and cell constants. *J Appl Cryst* 26:795–800.
10. Vagin A, Teplyakov A (1997) MOLREP: An automated program for molecular replacement. *J Appl Cryst* 30:1022–1025.
11. Murshudov GN, Vagin AA, Dodson EJ (1997) Refinement of macromolecular structures by the maximum-likelihood method. *Acta Crystallogr* D53:240–255.
12. Winn MD, Murshudov GN, Papiz MZ (2003) Macromolecular TLS refinement in REFMAC at moderate resolutions. *Methods Enzymol* 374:300–321.
13. Kuper J, Doenges C, Wilmanns M (2005) Two-fold repeated (betaalpha)4 half-barrels may provide a molecular tool for dual substrate specificity. *EMBO Rep* 6:134–139.
14. Wright H, et al. (2008) The structure/function relationship of a dual-substrate (betaalpha)8-isomerase. *Biochem Biophys Res Commun* 365:16–21.
15. Hommel U, Eberhard M, Kirschner K (1995) Phosphoribosyl anthranilate isomerase catalyzes a reversible amadori reaction. *Biochemistry* 34:5429–5439.
16. Eberhard M (1990) A set of programs for analysis of kinetic and equilibrium data. *Comput Appl Biosci* 6:213–221.

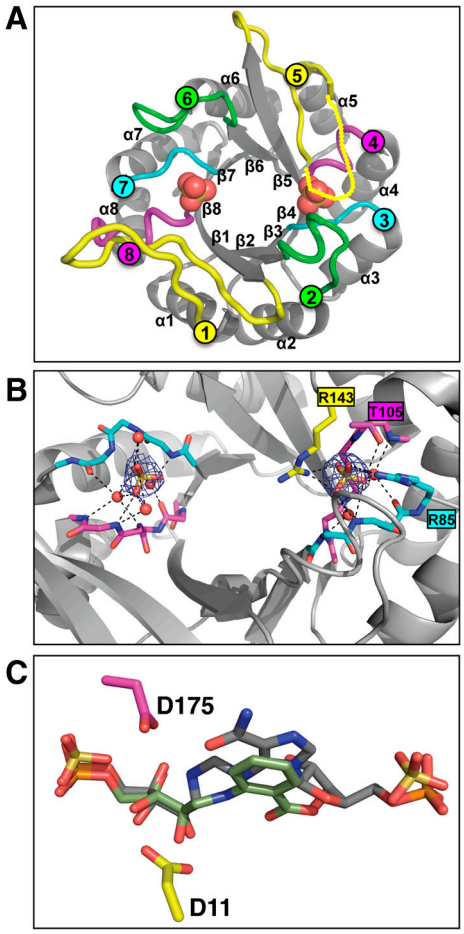

Fig. S1. Active site structure of PriA. (*A*) Ribbon representation of the PriA-sulfate (apo) structure. The eight active site loops 1–8 are colored in yellow (1,5), green (2,6), cyan (3,7), and magenta (4,8), emphasizing the twofold repeated $(\beta/\alpha)_4$ half-barrel elements. A disordered segment from loop 5 is indicated with a dashed line. The secondary structural elements that form the $(\beta/\alpha)_8$ barrel are labeled. (*B*) Active site structure of the PriA-sulfate complex. For further details, see Fig. 2. (*C*) Superposition of the ligands found in the crystal structures of the three PriA complexes. The ligands are shown in atom-specific colors, following the scheme of Fig. 2. The carbon atoms of rCdRP and PrFAR are in gray-green and gray, respectively. The positions of the two catalytic PriA residues, Asp11 and Asp175, are also shown.

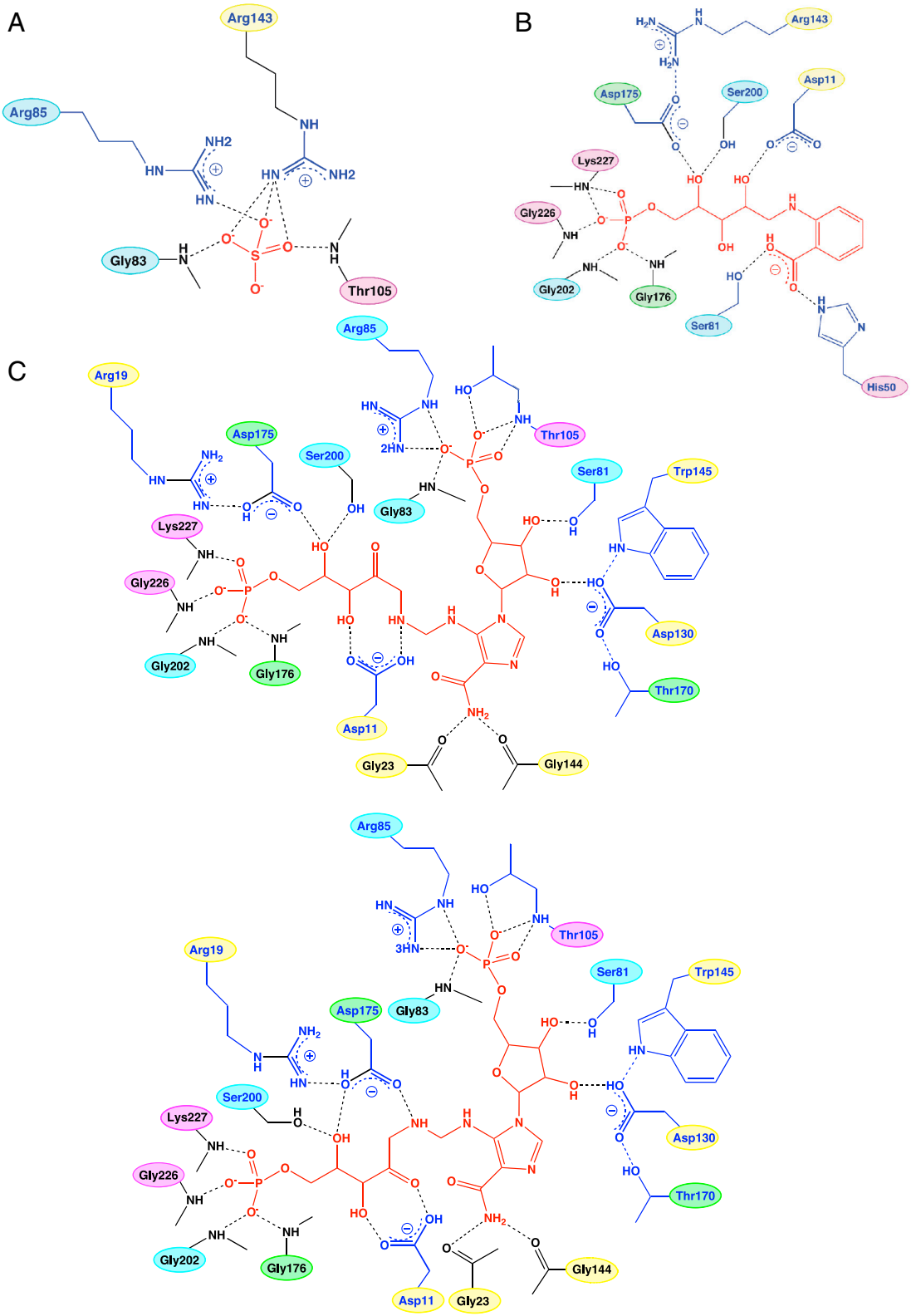

Fig. S2. Schematic presentation of specific hydrogen-bond PriA-ligand interactions. (*A*) First sulfate ion; (*B*) rCdRP; (*C*) PrFAR, first conformation; (*D*) PrFAR, second conformation. Color codes: ligands, red; PriA side-chain atoms involved in ligand interactions, blue; PriA main chain involved in ligand interactions, black. The colors of the residue labels follow the color scheme of Fig. 1. For reasons of clarity, water-mediated hydrogen bonds and van der Waals interactions are not displayed. The second sulfate ion is not included because all observed sulfate-PriA interactions are solvent mediated, except one direct hydrogen bond with the main chain carbonyl group of Val203 (cf. Fig. S1*B*).

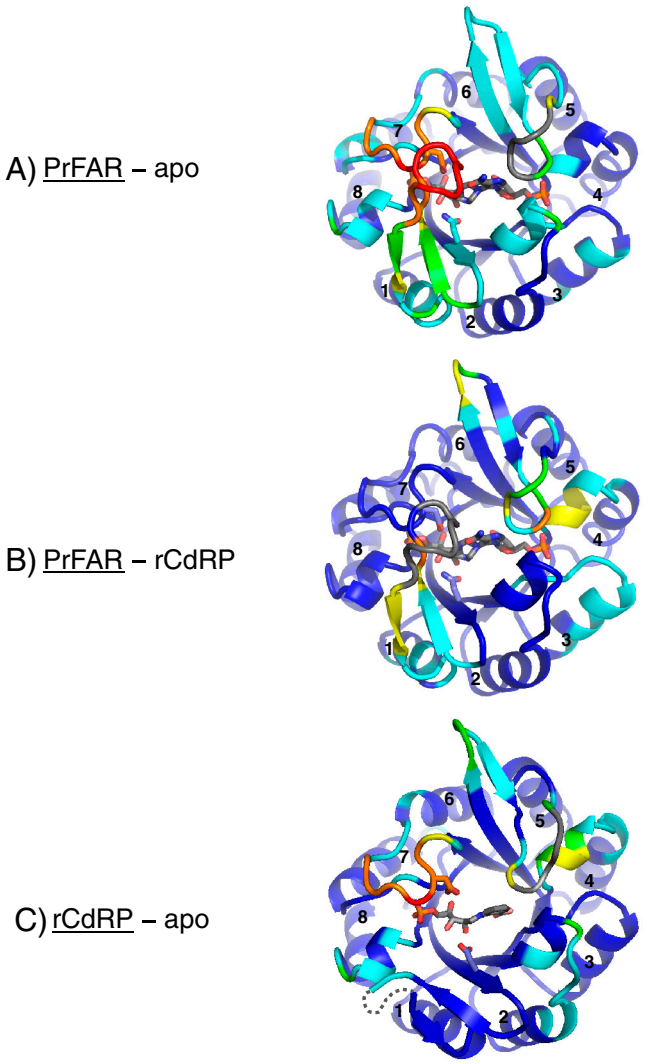

Fig. S3. Conformational changes observed by comparison of the three PriA-ligand complexes. The coordinate sets used for presentation are underlined. Color codes: blue, <1 Å; cyan <2 Å; green <3 Å; yellow <5 Å; orange <10 Å; red >10 Å; gray, no structural match. The spatial differences have been taken from the output of Secondary Structure Matching superpositions (1). For residue pairs where no structural superposition was possible, the distances between C_α atoms were measured.

1. Krissinel E, Henrick K (2004) Secondary-structure matching (SSM), a new tool for fast protein structure alignment in three dimensions. *Acta Crystallogr D* 60:2256–2268.

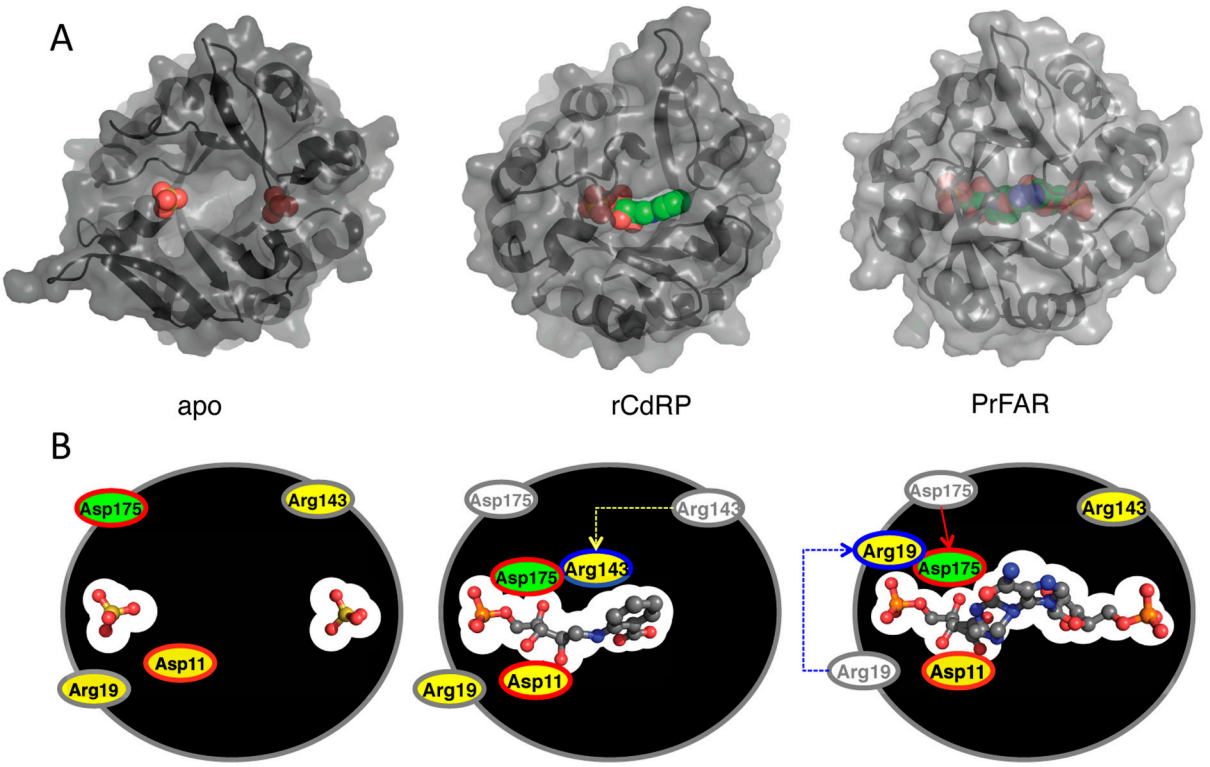

Fig. S4. Substrate-induced active site adaptation. (*A*) Variable active site sequestration in PriA: PriA-sulfate (apo) complex (*Left*), PriA-rCdRP complex (*Center*), and PriA-PrFAR complex (*Right*). The PriA structures are shown in combined ribbon and semitransparent surface presentation. The ligands, bound in each complex, are displayed as space-filling spheres, using the color conventions of Fig. 1. In the PriA apo-conformation, the active site is basically open and forms a deep cavity that can be recognized in the center of the structure. Whereas rCdRP is partly exposed to external solvent, PrFAR is entirely sequestered, due to major conformational changes of the PriA active site loop structure (cf. Fig. 1). (*B*) Schematic presentation of the variable active site structures of PriA, in the presence of sulfate (apo conformation, *Left*), rCdRP (*Center*) and PrFAR (*Right*). The ligands are shown in ball-and-stick presentation. The PriA catalytic residues Asp11 and Asp175, and the residues recruiting Asp175 into the active site (Arg19, Arg143), are displayed schematically. Observed movements of Arg19, Arg143, and Asp175 in the PriA complex structures with reaction ligands (rCdRP, PrFAR) are indicated by dashed lines. The color conventions are as in Fig. 1.

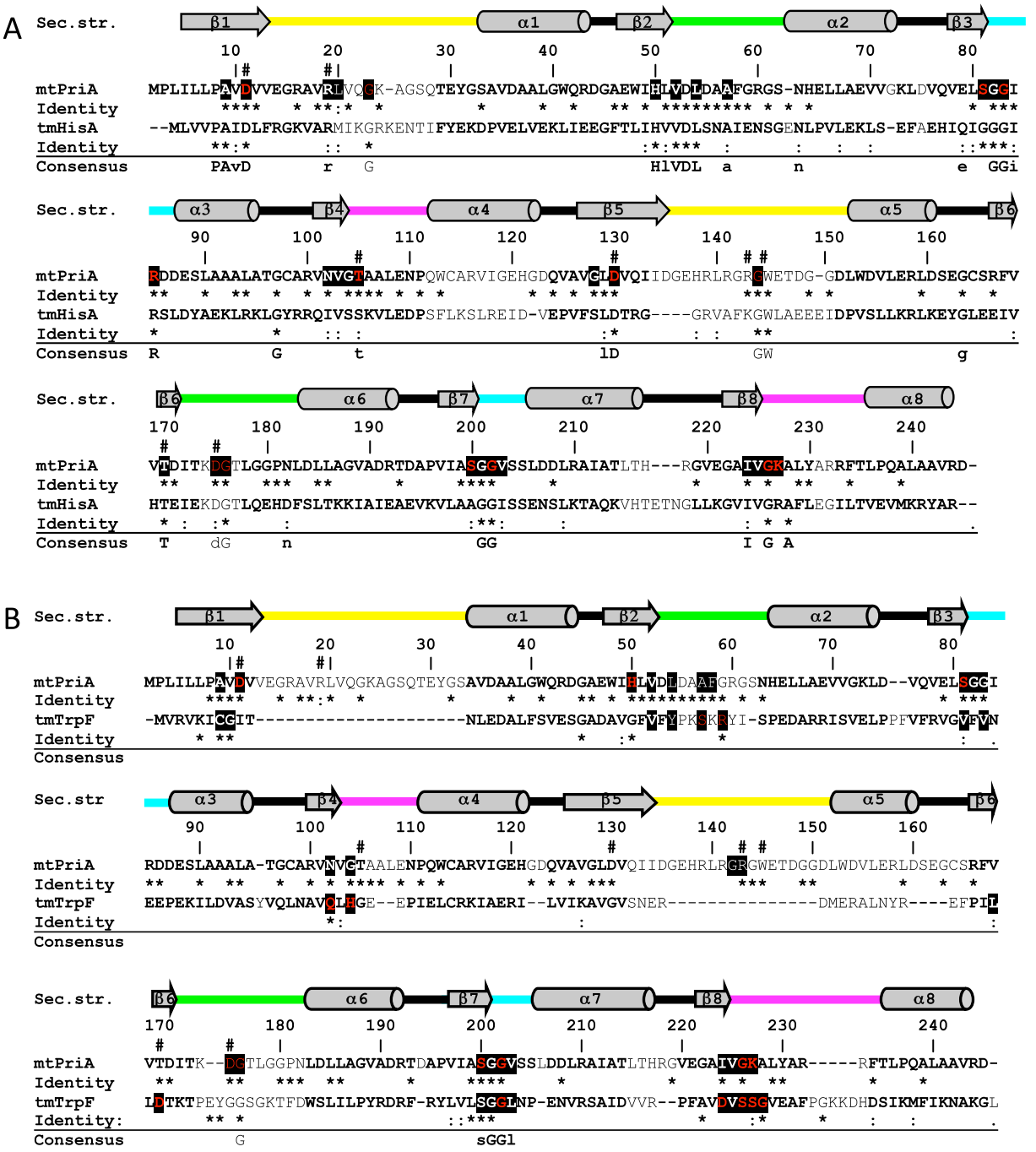

Fig. S5. Structure-based sequence alignment of (*A*) PriA/HisA and (*B*) PriA/TrpF. Those sequence segments that could be superimposed according to the criteria of SSM (1) are in bold; the remaining sequence parts are shown with regular characters. The locations of secondary structural elements for PriA, as determined by SSM, are indicated by symbols (α-helices, cylinders; β-strands, arrows). For clarity of presentation, only the canonical $(\beta/\alpha)_8$-barrel secondary structural elements are shown. The color codes of the active site loops follow the conventions of Fig. 1. Residue conservation for each sequence is indicated in lines marked as "Identity" by "*" (invariant) and ":" (invariant in at least 90% of all homologous sequences). The values have been taken from multiple sequence alignments of all unambiguously detectable PriA (30), HisA (102), and TrpF (99) sequences with correct functional annotations. Conservation across paralogous sequences is shown in the lines marked "Consensus." Please note that only in the PriA/HisA pair there are conserved residues across the entire sequences, whereas for the pair PriA/TrpF conservation is restricted to loop 7, which is involved in the formation of the conserved phosphate-binding site (2). Protein-ligand interactions are indicated by black boxes for PriA-PrFAR (*A*), PriA-rCdRP and TrpF-rCdRP (PDB ID code 1LBM) (*B*). For HisA, at present, there is no available structure of a ligand complex. Those residues that are involved in hydrogen-bond interactions (cf. Fig. S2) are in red. PriA residues that were mutated for biochemical characterization are indicated by "#" signs.

1. Krissinel E, Henrick K (2004) Secondary-structure matching (SSM), a new tool for fast protein structure alignment in three dimensions. *Acta Crystallogr D* 60:2256–2268.
2. Wilmanns M, Hyde CC, Davies DR, Kirschner K, Jansonius JN (1991) Structural conservation in parallel beta/alpha-barrel enzymes that catalyze three sequential reactions in the pathway of tryptophan biosynthesis. *Biochemistry* 30:9161–9169.

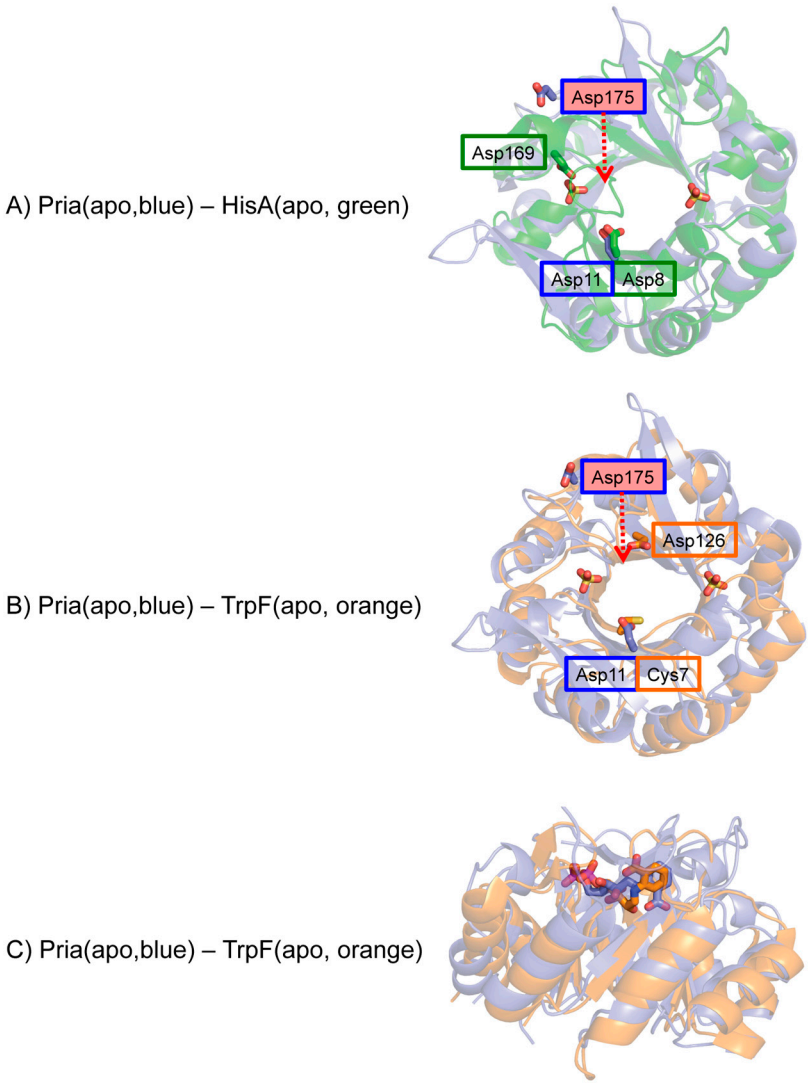

Fig. S6. Comparison of PriA bisubstrate catalysis and (*A*) HisA/(*B* and *C*) TrpF single-substrate catalysis. The apo conformations of the respective protein structures are shown as ribbons in different faint colors (PriA: 2Y89, blue; HisA: 1QO2, green; TrpF: 1NSJ, orange). The orientation is similar to that in Fig. 1. The base/acid catalytic residues (in one letter-code) are shown in stick presentation with atom-specific colors, in which the carbon atoms match the colors of the respective ribbons. The active site sulfate ions, found in the PriA apo structure, are shown in stick presentation with atom-specific colors as well. For the pair PriA/HisA, the catalytic residues are in structurally aligned positions (cf. Fig. S5*A*). Whereas Asp11(PriA)/Asp8(HisA) superimpose well, only the second catalytic HisA residue (Asp169) is oriented towards the active site, whereas the equivalent residue in PriA (Asp175) is outside the active site and therefore needs to be recruited into the active site upon substrate binding, as indicated by arrows, to participate in PriA catalytic activity (cf. Fig. 1 and Fig. S4*B*). In contrast, for the pair PriA/TrpF the two acid/base catalytic residues pairs, Asp11(PriA)/Cys7(TrpF) and Asp175(PriA)/Asp126(TrpF), are not in structurally matching sequence positions (cf. Fig. S5*B*). As for HisA, both TrpF catalytic acid/base residues are located within the active site and hence do not need to be recruited. (*C*) Side view of the PriA-rCdRP complex, superimposed on the TrpF-rCdRP complex (PDB ID code 1LBM). While in PriA-rCdRP complex the anthranilate carboxylate group of rCdRP is oriented toward the throat of the PriA active site and is hydrogen bonded to His50 and Ser81 (Fig. 2 and Fig. S2*B*), the same group in the TrpF-rCdRP complex (PDB ID code 1LBM) is oriented toward the external solvent.

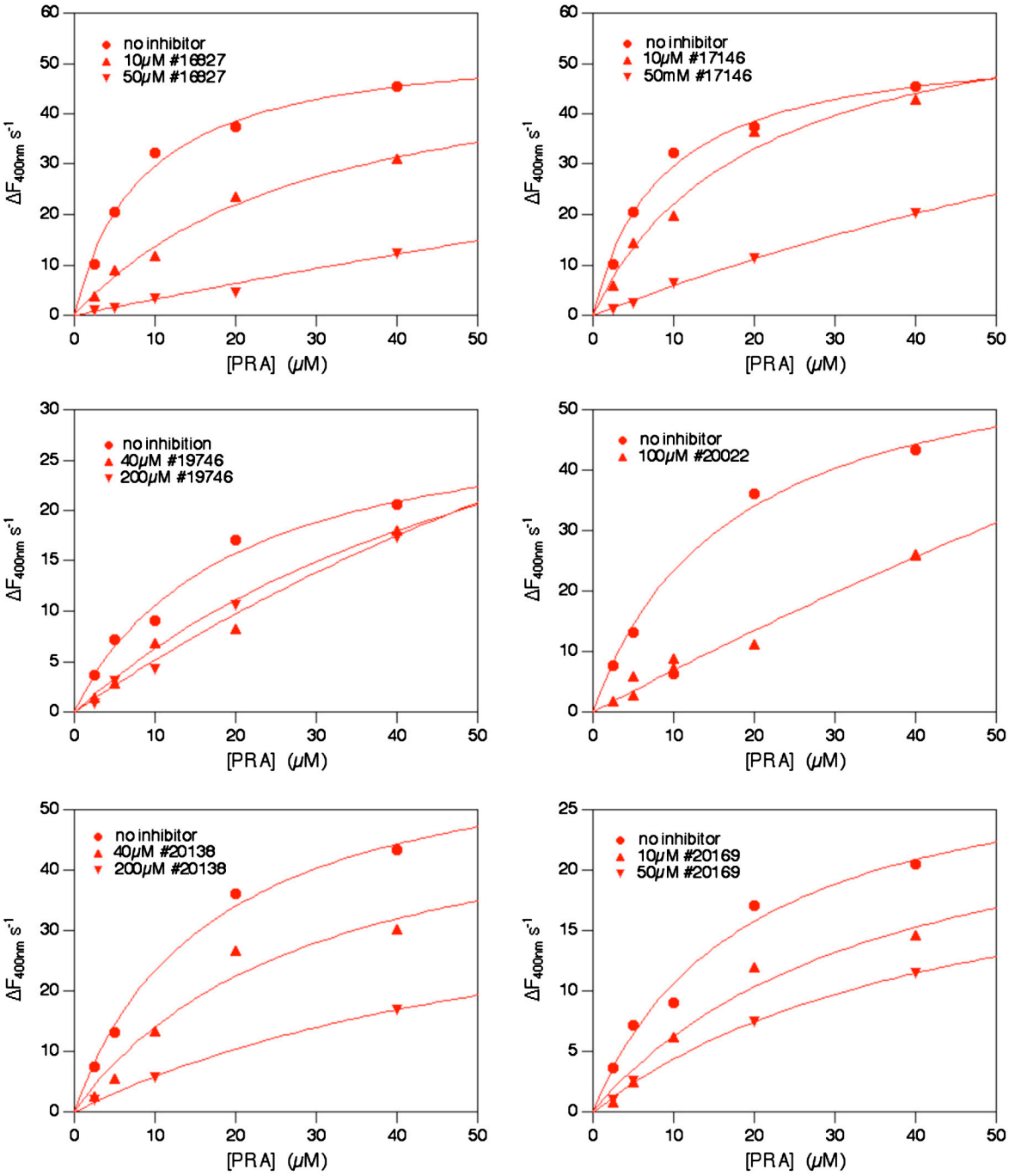

Fig. S7. Inhibition patterns of PriA inhibitors in PRA isomerization. The initial rates of the PRA isomerization reaction by PriA was determined in the presence of different concentrations of six PriA inhibitors. The obtained data for each individual inhibitor concentration were fitted to the equation for Michaelis–Menten kinetics. The patterns for the different inhibitors with those for competitive inhibition. The inhibition constants (K_i^{PRA}) were determined by fitting the data simultaneously to the equation for competitive inhibition.

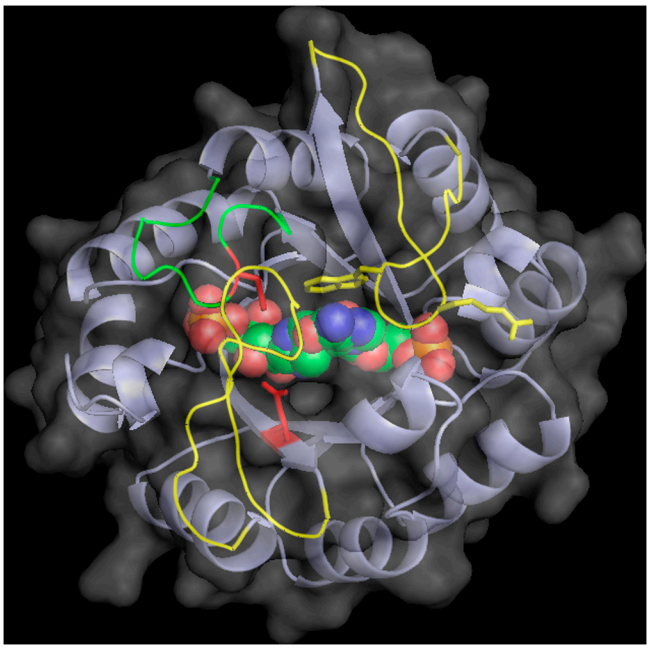

Movie S1. Conformational changes from the PriA apo structure (start) to the rCdRP bound (tryptophan biosynthesis) structure (end) in semitransparent surface/ribbon presentation. The positions of the catalytic residues Asp11 and Asp175 are highlighted in red, and those of loops 1, 5 (including residues Arg143 and Trp145), and 6 are in colors that are used in Fig. 1. The rCdRP molecule is shown in sphere presentation, using atom-specific colors.
Movie S1 (MOV)

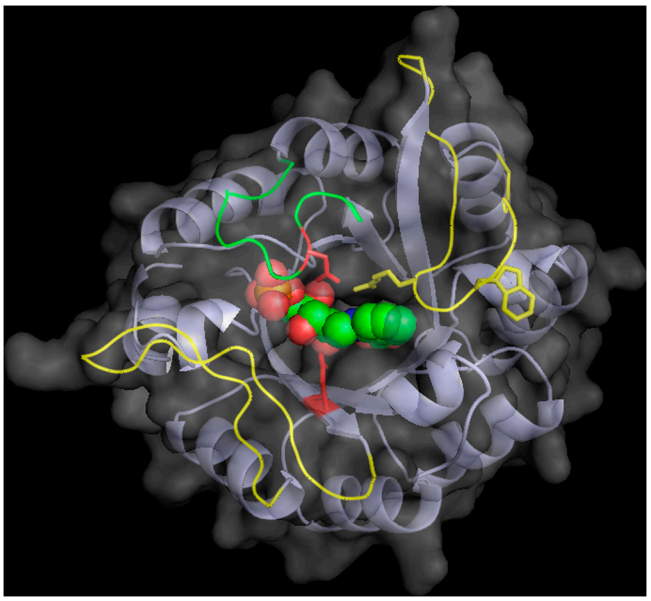

Movie S2. Conformational changes from the PriA apo structure (start) to the PrFAR bound (histidine biosynthesis) structure (end). The color codes of structural elements highlighted are as in Movie S1.
Movie S2 (MOV)

Table S1. X-ray structure determination

	PriA(D11N)-apo	PriA(WT)-rCdRP	PriA(D11N)-PrFAR
PDB ID code	2Y89	2Y85	2Y88
X-ray data statistics			
Wavelength (Å)	0.801	0.978	0.801
Max. resolution (Å)	2.5	2.4	1.33
Space group	$P4_332$	$P2_1$	$P4_32_12$
Unit cell dimensions	$a = 141.5$ Å	$a = 46.0$ Å $b = 121.1$ Å $c = 81.1$ Å $\beta = 95.6^o$	$a = 63.3$ Å $c = 131.2$ Å
No. of reflections	17,377	34,409	61,458
Completeness*	100.0 (100.0)	99.9 (99.9)	99.1 (95.8)
Redundancy*	14.1 (14.4)	3.8 (3.8)	8.4 (7.4)
R_{sym}*,†	0.11 (0.72)	0.13 (0.46)	0.04 (0.58)
$I/\sigma I$*,‡	23.9 (3.1)	9.1 (3.2)	31.2 (3.4)
Refinement statistics			
Resolution limits (Å)	25–2.5	30–2.4	20–1.33
No. of reflections	16,459	32,627	58,387
R_{cryst}/R_{free}§	0.21/0.25	0.21/0.29	0.14/0.18
Numbers of atoms refined			
Protein atoms	1,743	6,920	1,878
Ligand atoms	35	100	37
Solvent atoms	128	188	394
Average B factors in Å²			
Protein atoms	36	31	18
Ligand atoms	59	34	16
Solvent atoms	36	24	32

*Numbers in parentheses correspond to the highest resolution shell.

†$R_{sym} = \sum_{hkl}\sum_i |I_i - \langle I\rangle| / \sum_{hkl}\sum_i I_i$, where I_i is the ith measurement and $\langle I\rangle$ is the weighted mean of all measurements of I.

‡$\langle I\rangle/\langle\sigma I\rangle$ indicates the average of the intensity divided by its average standard deviation.

§$R_{cryst} = \sum_{hkl}||F_o| - |F_c|| / \sum_{hkl}|F_o|$, where F_o and F_c are the observed and calculated structure factor amplitudes, respectively. R_{free} is equivalent to R_{cryst} , calculated from 5% of the diffraction data that were randomly omitted from refinement. The total number of reflections includes the R_{free} subset.

Table S2. Steady-state kinetics for ProFAR and PRA isomerization of PriA variants

	K_M^{ProFAR} [M]	k_{cat} [s^{-1}]	k_{cat}/K_M^{ProFAR} [$M^{-1}\,s^{-1}$]	K_M^{PRA} [M]	k_{cat} [s^{-1}]	k_{cat}/K_M^{PRA} [$M^{-1}\,s^{-1}$]
Wild-type	$1.9 \pm 0.3 \times 10^{-5}$	$2.3 \pm 0.1 \times 10^{-1}$	1.2×10^4	$2.1 \pm 0.2 \times 10^{-5}$	3.6 ± 0.6	1.7×10^5
D11A	ND	ND	ND	ND	ND	ND
D11N	$1.0 \pm 0.5 \times 10^{-4}$	$5.0 \pm 0.9 \times 10^{-4}$	5.0	$5.0 \pm 0.3 \times 10^{-5}$	$2.7 \pm 0.4 \times 10^{-3}$	5.4×10
R19A	$1.7 \pm 0.2 \times 10^{-4}$	$7.1 \pm 0.4 \times 10^{-2}$	4.1×10^2	$3.1 \pm 0.2 \times 10^{-5}$	1.0 ± 0.1	3.3×10^4
T105A	ND	ND	ND	$2.7 \pm 0.3 \times 10^{-5}$	$3.5 \pm 1.1 \times 10^{-1}$	1.3×10^4
T105V	ND	ND	ND	$2.0 \pm 0.1 \times 10^{-5}$	$3.7 \pm 0.3 \times 10^{-1}$	1.8×10^4
D130A	$1.7 \pm 0.5 \times 10^{-5}$	$1.0 \pm 0.1 \times 10^{-2}$	6.0×10^2	$1.6 \pm 0.5 \times 10^{-5}$	1.4 ± 0.4	9.1×10^4
R143A	ND	ND	2.4×10^2	ND	ND	6.0×10^3
R143K	ND	ND	6.7×10^2	ND	ND	1.3×10^3
W145A	ND	ND	ND	$3.7 \pm 0.3 \times 10^{-5}$	2.2 ± 0.3	5.8×10^4
W145F	$7.1 \pm 1.1 \times 10^{-5}$	$4.4 \pm 1.0 \times 10^{-3}$	6.2×10	$3.4 \pm 0.4 \times 10^{-5}$	2.2 ± 0.2	6.3×10^4
T170A	$1.5 \pm 0.1 \times 10^{-4}$	$3.9 \pm 0.9 \times 10^{-2}$	2.7×10^2	$1.7 \pm 0.1 \times 10^{-5}$	$5.5 \pm 0.4 \times 10^{-1}$	3.3×10^4
D175A	ND	ND	ND	ND	ND	ND
D175N	$2.4 \pm 0.5 \times 10^{-5}$	$9.0 \pm 0.7 \times 10^{-4}$	3.7×10	$7.1 \pm 1.0 \times 10^{-6}$	$6.5 \pm 0.9 \times 10^{-2}$	9.2×10^3